applied sciences

MDPI

Article

Investigation of FDM-Based 3D Printing for Optimized Tooling in Automotive and Electronics Sheet Metal Cutting

Szabolcs Szalai [1], Brigitta Fruzsina Szívós [1], Vivien Nemes [1], György Szabó [1], Dmytro Kurhan [2], Mykola Sysyn [3] and Szabolcs Fischer [1,*]

[1] Central Campus Győr, Széchenyi István University, H-9026 Győr, Hungary; szalaisz@sze.hu (S.S.); szivos.brigitta.fruzsina@sze.hu (B.F.S.); nemes.vivien@ga.sze.hu (V.N.); gyorgyszabo86@gmail.com (G.S.)
[2] Department of Transport Infrastructure, Ukrainian State University of Science and Technologies, UA-49005 Dnipro, Ukraine; d.m.kurhan@ust.edu.ua
[3] Department of Planning and Design of Railway Infrastructure, Technical University Dresden, D-01069 Dresden, Germany; mykola.sysyn@tu-dresden.de
* Correspondence: fischersz@sze.hu; Tel.: +36-(96)-503-400

Abstract: Within the scope of the work, the possible use of fused deposition modeling (FDM) technology in executing rapid prototypes of cutting tools for aluminum sheets was systematically studied. Relevant investigations have thus far mainly concentrated on tools for the 3D printing of bent and deep-drawn pieces, yet the implementation of FDM tools in cutting has been insufficiently covered. This study aims to determine the characteristics of FDM cutting tools, such as wear and tear, dimensional stability, and cutting efficiency. Various tool designs were tested under different wall thicknesses and orientations with respect to the feed of Al99.5 sheets with thicknesses of 0.22 mm and 0.3 mm. According to the results, in the best case, three-dimensional printed PLA tools performed six cuts with no burrs and an acceptable wear level due to the IT tolerances (IT9 and IT10). Tools with thicker walls and more appropriate orientations were found to be more robust. However, some designs failed when subjected to greater loads, revealing a deficiency in some of the strength properties of the material. These observations suggest that it is possible to create 3D printed tools for modeling and small-scale production at considerably cheaper and faster rates than conventional methods. Future work will integrate advanced materials and designs to enhance tool performance, further solidifying FDM as a transformative approach in industrial tool manufacturing. With this research, the authors wanted to demonstrate that FDM technology can also be used to produce a classic sheet cut, which, of course, is still of great importance for prototyping or setting up production processes. This research demonstrated that FDM printing can play a role in this area.

Keywords: 3D printing; PLA; FDM; rapid prototype; 3D scanning; optimization; part-off die; cut-off die; GOM ATOS; sheet metal

Academic Editor: Manoj Gupta

Received: 30 November 2024
Revised: 30 December 2024
Accepted: 3 January 2025
Published: 6 January 2025

Citation: Szalai, S.; Szívós, B.F.; Nemes, V.; Szabó, G.; Kurhan, D.; Sysyn, M.; Fischer, S. Investigation of FDM-Based 3D Printing for Optimized Tooling in Automotive and Electronics Sheet Metal Cutting. *Appl. Sci.* **2025**, *15*, 442. https://doi.org/10.3390/app15010442

1. Introduction

Sheet metal forming is widely used across various industries and is one of the most popular manufacturing technologies to produce finished products [1–4]. Its applications are especially prominent in the automotive and aerospace industries, as well as in the food and domestic appliance sectors [5,6]. Key advantages of this technology include the ability to produce parts without requiring highly skilled labor, as well as its ease of production, excellent mechanical properties of the formed parts, and minimal waste generation. However, its major drawbacks include the high cost of tooling, the

extended time needed for tool production, and the lengthy iterative process to achieve the final geometry [1–4]. This iterative process can significantly delay the optimization of tooling production [7,8].

In today's industries, rapid product development is crucial for maintaining competitiveness [9–12]. Flat sheets can be transformed into complex three-dimensional components using processes such as bending and deep drawing [2,13]. Advanced operations include welding [14], bolting, adhesive bonding [15], and the use of clips [16,17], among others. There is a growing demand for customized components and small-batch production. Rapid prototyping presents a significant opportunity to reduce both product development time and manufacturing costs [5–8]. Tooling processes that allow sheet metal forming without relying on conventional (metal) tools are increasingly important, particularly for short production runs where conventional tooling costs are prohibitive. Prototyping aims to optimize manufacturing processes and detect potential defects.

Due to the high production time and cost of conventional tools, sheet metal-forming technology is primarily suitable for large-scale production. To address this, the use of additively manufactured tools and alternative materials, such as aluminum and synthetic resins, has gained attention. Additive manufacturing offers greater flexibility and resource savings, making it ideal for rapid prototyping and low-volume production. Market demand has driven significant interest in additive manufacturing technologies and 3D printing [18–21].

3D printing is rapidly advancing, enabling the production of complex parts that are challenging to create using other methods. This process starts with a digital CAD file that is converted into an STL format. Specialized slicing software generates a G-code file containing layer-specific instructions, which the 3D printer uses to create the part layer by layer [22–24]. Similar technologies have been applied to unique applications, such as 3D printing railway ballast aggregates [25,26] and studying ballast track deformation [27,28].

Various polymeric materials have proven valuable in the development of sheet-forming tools, particularly for low-volume production, offering significant cost savings and shorter lead times [20,29]. PLA (polylactic acid) is a popular and inexpensive 3D printing material with excellent printability. Research has shown that 3D-printed PLA tools can effectively shape sheet metal, delivering results comparable to those achieved with metal tools in terms of formability [9,30].

From a tooling perspective, fused deposition modeling (FDM) is one of the most promising 3D printing technologies. Studies highlight significant potential for the use of FDM tools across various industries. This technology builds parts by depositing layers of molten plastic. While the raw material (plastic filament) is cost-effective, the resulting parts exhibit lower strength compared to those made via conventional injection molding due to slight porosity [1,18].

FDM plastic tools in sheet metal forming offer shorter lead times than conventional tooling. However, due to their lower yield strength and elastic modulus, plastic tools are more prone to failure and have reduced dimensional accuracy. Therefore, these tools are most suitable for small-batch production, where their manufacturing cost is significantly lower than that of traditional metal-forming tools. Additionally, the elastic deformation of plastic tools reduces friction during forming, eliminating the need for the surface treatments required for metal tools [1,18].

Because tooling is typically expensive and initial tool tests are often imperfect due to the complexity of modern parts and sheet materials, 3D-printed tools provide an attractive alternative for rapid prototyping and small-scale production [2,18]. Although extensive research exists on 3D-printed polymer tools for bending and deep drawing, studies on their use in cutting or punching applications remain scarce [2,13].

Various studies have examined the feasibility of using 3D-printed tools for sheet metal forming. Conventional metal tools are dominant in the sheet metal bending sector, but unfilled and reinforced plastics are being explored as cost-effective alternatives to replace metal components [2,19]. Additionally, thermoplastics are recyclable, and polymer tool inserts produced via 3D printing or other rapid manufacturing methods can be quickly replaced. Polymer inserts have also been shown to reduce aesthetic defects in bent sheets. Studies indicate that in air bending, polymer tool inserts achieve comparable process capabilities to those of metal tools [2,19].

Research into using 3D-printed tool inserts in metal frames for V-bending has shown that springback behavior is comparable to that of all-metal tools. Additionally, using plastic tools improves surface quality due to reduced scratching of the workpiece [2,19]. When all-plastic tools were tested for V-bending, the final bending angle exhibited lower accuracy due to increased elastic deflection. However, the process showed repeatable performance across different materials [2,31].

Challenges in using thermoplastics for punching applications include their low compressive strength and variability in the manufacturing process caused by 3D printing parameters. Researchers have identified critical printing parameters, such as infill percentage, wall thickness, extrusion width, and printing temperature. Experiments on deep drawing demonstrated that cups could be successfully formed without visible wear on 3D-printed tools [1,2]. Furthermore, lubrication was found to be unnecessary for forming heat exchanger plates when using plastic tools, thanks to the plastic's anti-friction properties [2].

FDM tools have also been used for 90° bending tasks. Despite the low strength of plastic tools, they successfully bent sheets, including steel plates, with tensile strengths of up to 440 MPa. However, enhancing tool stiffness is necessary to improve dimensional accuracy [18]. Experiments on deep drawing with plastic dies revealed that high-pressure conditions caused the tools to deform permanently, making them unsuitable for further use [18].

The environmental issues associated with lubricants in metal forming emphasize the importance of developing lubrication-free processes. Plastic tooling has been shown to prevent sticking, a common issue with steel tooling during extrusion [18]. Research combining PLA dies with steel stamps showed that this approach effectively improved the dimensional accuracy of bent parts for both aluminum and steel sheet metals [9,32].

A consistent theme across the literature is that 3D printing is well-suited for rapid prototyping and the small-scale production of forming tools [2]. Efforts to enhance the mechanical properties of 3D-printed tools have focused on optimizing parameters such as layer thickness, orientation, and infill structure. The anisotropic nature of FDM parts significantly affects their strength and stiffness, with the stronger/strongest properties aligned along the extrusion direction [33–35].

Dimensional accuracy, influenced by parameters like extrusion temperature, feed rate, and nozzle diameter, is critical for practical applications. Higher extrusion temperatures can lead to dimensional deviations due to material expansion, while optimized slicing software and machine controls have been shown to improve accuracy [36–39].

In summary, while FDM technology has found widespread applications, its potential for cutting applications in sheet metal forming remains largely unexplored. This study aimed to investigate the use of 3D-printed cutting tools, detailing materials, methods, results, and conclusions. Future research will explore further applications and improvements.

2. Materials and Methods

This section describes the materials used, the equipment needed for the experiments, and the test procedure.

2.1. Materials

In the experiment, Al99.5 sheet materials with thicknesses of 0.22 and 0.3 mm were tested for cutability. Al99.5 is a high-purity aluminum alloy with a 99.5% aluminum content and is one of the most commonly used materials in the aluminum industry. Due to its high purity, it has many favorable properties that make it suitable for various industrial, and even architectural, applications. It is used as a raw material for switches, contacts, and other electrical components in the automotive industry. It is used for exterior cladding and roof tiles in the construction industry due to its corrosion resistance. It is resistant to corrosion in acidic or alkaline environments and is therefore used in tanks suitable for the storage of chemicals. It is also used in automotive cooling and heating systems. It is precisely because of this broad applicability, which the authors experience in their own daily work, that the authors conducted this study.

Al99.5 has excellent corrosion resistance to a wide range of environmental influences, such as atmospheric, water, and chemical attacks. This makes it particularly suitable for outdoor applications and environments where corrosion protection is critical. The material has excellent formability in both cold and hot conditions. Al99.5 sheets can be easily formed into different shapes by, for example, bending, rolling, or pressing. It is, therefore, often used in applications where precise and easy formability is essential. In the automotive and electronics industries, it is used prominently for bulbs and fluorescent tube housings. Table 1 summarizes the measured chemical composition of the Al 99.5 material.

Table 1. Measured chemical composition of the Al99.5 in w/w% unit (ISO 209 [40]).

Cu	Mg	Mn	Si	Fe	Zn	Ti	Al
0.05 max.	0.05 max.	0.05 max.	0.25 max.	0.40 max.	0.07 max.	0.05 max.	99.5 min.

Al99.5 has a relatively low strength compared to other aluminum alloys, making it unsuitable for structural components requiring high mechanical stress. However, its low density and good ductility make it an excellent material for lightweight but strong structures. Table 2 illustrates the measured mechanical properties of the AL 99.5 material.

Table 2. Measured mechanical properties of the Al99.5 [41,42].

Measured Mechanical Properties	
Tensile strength [MPa] ISO 6892	60
0.2% proof strength [MPa] ISO 6892	20
Min. elongation at fracture [%] ISO 6892	25
Brinell hardness [HBW] ISO 6506	20

Filaticum PLA filament was chosen to 3D print the cutting tools, as it provides excellent printing parameters. It was also chosen because it is a common, easily available, easy to print, non-specialized 3D printing material, which will enhance the results of the tests by proving the applicability of the cheapest possible solution needed to generate a successful test. Filaticum PLA is a type of composite material that contains other ingredients besides PLA, such as pigments, lubricants, and fillers, which result in a “softer” PLA. This makes the filament easy to print, even at lower temperatures. Another favorable property of Filaticum PLAs is that they shrink only minimally, resulting in no deformation of the printed piece, which is particularly important for various tooling applications. The filaments are made from natural raw materials and are biodegradable under industrial conditions, making them excellent for prototypes and various models. Table 3 shows the main parameters of the PLA budget. PETG and ABS were deliberately not used because one of the aims of the

article was to investigate PLA material that can be printed well with the simplest printing parameters and using cheap printers.

Table 3. PLA budget filament parameters.

Filaticum	PLA Budget
Nozzle temperature [°C]	195–225
Nozzle size [mm]	0.2–1.2
Bed temperature [°C]	max. 70
Cooling fan [%]	recommended up to 100
Layer height [mm]	0.2–0.8
Print speed [mm/s]	optimal 20–80, max. 250

Table 4 shows the mechanical properties of the material according to the different standards.

Table 4. Raw material mechanical properties [43–47].

Physical Properties	Method	PLA
Specific gravity [g/cm^3]	D792	1.24
Heat distortion temp. (HDT) [°C]	D790	55
Glass trans. temp [°C]	D3418	55–60
Tensile strength [MPa]	ISO 527	60
Tensile elongation [%]	ISO 527	6.00
Tensile modulus [MPa]	ISO 527	3800
Notched Izod impact [kJ/m^2]	ISO 180	16

2.2. Equipment

The test pieces were printed on the Creality CR-10S Pro V2 3D printer (Shenzhen Creality 3D Technology Co., Shenzhen, China). The printer has a large print volume (300 × 300 × 400 mm), which allows for the production of larger objects. The device is equipped with a number of advanced features, including automatic leveling, which significantly simplifies print preparation. The printer features an improved extruder system that ensures more uniform material feed and minimizes jams, improving print reliability. Table 5 summarizes the most important parameters of the printer.

Table 5. Creality CR 10S Pro V2 data sheet.

Printer	Creality CR 10S Pro V2
Technology	Fused deposition modeling (FDM)
Build volume [mm]	$X \times Y \times Z$: 300 × 300 × 400
Filament diameter [mm]	1.75
Feeder type	dual drive (DD)
Max. hot end temperature [°C]	260
Max. heated bed temperature [°C]	100
Max. print speed [mm/s]	180
Slice thickness [mm]	0.1–0.4
Print precision [mm]	±0.1

The CR-10S Pro V2 is equipped with a touchscreen and TMC 2208 motor controller for virtually silent operation. The heated print bed heats up quickly, and the printer is compatible with a wide range of materials, including PLA, ABS (acrylonitrile butadiene styrene), PETG (polyethylene terephthalate glycol-modified), and TPU (thermoplastic polyurethane). The printer supports a restart function in the event of a power failure, so interrupted print runs can be resumed. With features like these, the CR-10S Pro V2 is a reliable, accurate, and versatile choice for general users. Figure 1 shows the printer and the printing orientation of the tools.

Figure 1. Illustration of printing layouts. (From the bottom up: the first row is tilted at 0°, the second at 15°, and the third at 45°).

Ultimaker Cura printer software (slicer) was used to set the printing parameters of the 3D printer. Cura is an open-source, accessible 3D printing software. Its primary purpose is 3D model slicing, i.e., to break down digital models into layers from which the 3D printer gradually builds the final object. Cura is widely used, as it is compatible not only with Ultimaker printers but also with many other brands and models.

The software's simple user interface and numerous configuration options make it attractive for beginners and advanced users alike. It offers a variety of modes: the default mode allows simple settings for fast printing, while advanced settings allow detailed control over layer thickness, print speed, and extrusion rate. It also supports the installation of plug-ins so that someone can add additional features, such as predictions of print time and material consumption. Table 6 contains the 3D printing properties, as well as Figure 2 shows the status of tools after slicing in Cura's software. It is important to note that the infill effect is being investigated in another study, where a 40% infill was chosen based on previous experience. In addition to examining the effect of orientation, the present study also investigates the effect of wall thickness.

Table 6. 3D printing properties (on the basis of [23,37,38]).

Properties of 3D Printing	
Nozzle temperature [°C]	215
Bed temperature [°C]	60
Print speed [mm/s]	50
Layer height [mm]	0.2
Infill [%]	40
Infill pattern	Cubic
Wall thickness [mm]	2, 4, and 6

The GOM ATOS II Triple Scan optical 3D coordinate measuring machine was used to determine the deformation of the tools (see Figure 3) by applying the DIC (digital image correlation) technique. The optical scanner(GOM GmbH, Braunschweig, Germany) was developed by GOM Software Co. (now Zeiss Inspect). The measuring system is based on structured light. With GOM ATOS II Triple Scan technology, it is possible to digitize the surface of objects of different sizes and to determine their coordinates by changing the

lenses of the cameras and projector and by changing the angle between the cameras. Its principle of operation is based on triangulation, which allows information about the whole geometry to be obtained. By automating the measurement process, the time required for the process is significantly reduced, making it more economical, and the accuracy of the inspection is increased, making it more and more widely used in various industries [27].

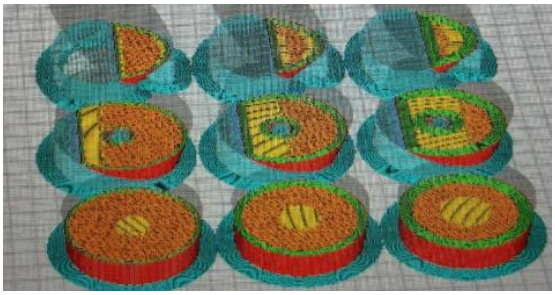

Figure 2. Tool orientation in Ultimaker Cura software. (From the bottom up: the first row is tilted at 0°, the second at 15°, and the third at 45°).

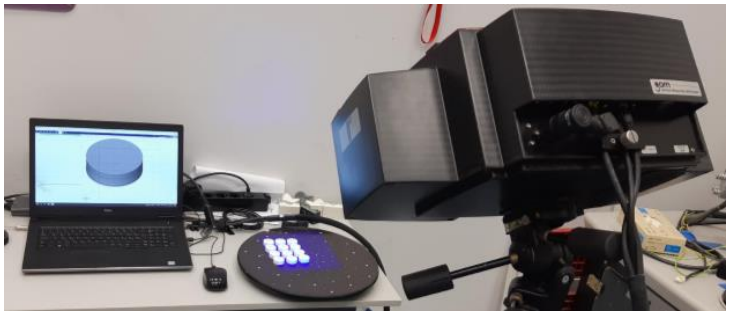

Figure 3. The GOM ATOS 3D scanner during digitization.

As a result of digitization, a dense, high-resolution point cloud in the software provides rapid feedback on individual defects, which has a positive impact on the production process. Non-contact measurement has a significant advantage over traditional tactile measurement in that a large number of measuring points can be recorded in a very short time [27].

In this research, MV170 lenses, i.e., the measuring range, were used to perform the measurements (Figure 3). Digitizing requires calibrating the system, which consists of scanning the caliper plate from different distances and angles. After the measurement, the measured models were compared with the CAD model of the initial piece in ATOS Professional 2017 software [27].

The Wimmer Garage Tools SP100E (see Figure 4) is a heavy-duty, 100-tonne workshop press specifically designed for use in industrial environments. This hydraulic press is the ideal solution for a variety of workshop tasks, including pressing, bending, forming, and other assembly tasks. The robust steel construction of the SP100E ensures its long life and a stable operation environment, while the hydraulic system provides precise and smooth force applications, making it easy for the user to handle challenging workflows. Its ergonomic design and simple control panel ensure ease of use, making it easy to use for both experienced professionals and less experienced users. The Wimmer Garage Tools SP100E is a reliable choice for any workshop where efficient and safe pressing is a priority. For technical specifications of the press, see Table 7.

Figure 4. The EZ-TOOLS SP100E workshop press.

Table 7. Az EZ-TOOLS SP100E data table.

Technical Specifications/Parameters	
Type/model	SP100E
Max. loading capacity [t]	100
Stroke length [mm]	approx. 280
Piston size in diameter [mm]	68
Maximum working width [mm]	810
Working height [mm]	approx. 60–950
Minimum height [mm]	approx. 400
Overall dimensions (length × width × height) [cm]	195 × 115 × 50
Height adjustment	at 7 points
Shipping dimension (length × width × height) [cm]	200 × 115 × 52
Shipping weight [kg]	630

2.3. The Cutting Process of the Specimens

To minimize burr formation, the correlation established by Komarov can be utilized during the design of the polyurethane-padded tool to determine the minimum height of the cutting edge that ensures optimal burr formation [48]. This relationship is illustrated in Figure 5.

Figure 5. Calculation method of the tool height (H) considering the conical angle (α).

The optimal height of the cutting die (H) to minimize burr formation can be calculated using Equation (1).

$$H = 3\left(1 + \frac{A_{11.3}}{100}\right)\sqrt{s}\ [\text{mm}] \quad (1)$$

where s is the thickness of the plate (sheet) in mm and $A_{11.3}$ is the percentage strain at breakage related to $L_o = 10{\cdot}d_0$, measuring the basis (base) length (d_0 represents the original diameter (or thickness) of the sample or specimen used in the tensile test before any deformation occurs) [49,50].

Using the Komarov tooling arrangement [48], the compression tools are commercially available 5 mm thick rubber sheets (80 ShoreA) stacked 50 mm thick. The cutting speed was not relevant due to the compression of the bases, but the machine speed was 20 mm/min.

Based on this correlation, the required cutting edge heights for the Al99.5 sheet materials with thicknesses of 0.22 mm and 0.3 mm are listed in Table 8. No literature data is available on the angle of under-grinding, and arbitrary values are generally recommended. For the experiments, a uniform under-grinding angle of 3° was applied.

Table 8. Tool height dimensions (on the basis of [1,18]).

H [mm]	
s	Al99.5 ($A_{11.3}$ = 50%)
0.22 mm	2.11
0.30 mm	2.46

The printing orientation (i.e., the angle between the printed object and the printing bed) can influence the mechanical properties of the model. To investigate this effect, the cutting edges for the polyurethane-padded punching tool were printed with three different orientations: 0°, 15°, and 45° relative to the plane of the print bed.

Adjusting the wall thickness can also affect the mechanical properties of the model. Increasing the wall thickness makes the model progressively stiffer. For the cutting edges of the polyurethane-padded punching tool, three wall thickness values were set for each printing orientation, aiming to determine the optimal configuration for punching thin aluminum sheets. These wall thicknesses were set to 2 mm, 4 mm, and 6 mm, as shown in Table 9.

Table 9. The measurement matrix.

Model	Sheet Thicknesses [mm]	Material	Orientation	Wall Thickness [mm]
A1	0.22; 0.3	Al99.5	0°	2
A2	0.22; 0.3	Al99.5	0°	4
A3	0.22; 0.3	Al99.5	0°	6
B1	0.22; 0.3	Al99.5	15°	2
B2	0.22; 0.3	Al99.5	15°	4
B3	0.22; 0.3	Al99.5	15°	6
C1	0.22; 0.3	Al99.5	45°	2
C2	0.22; 0.3	Al99.5	45°	4
C3	0.22; 0.3	Al99.5	45°	6

After printing, the brim (a technological addition to enhance adhesion) had to be removed from the edges of the printed tools. This feature improves adhesion to the printer bed. Furthermore, the supports had to be removed from the underside of tools printed at 15° and 45° orientations. These supports were necessary to provide backing for the initial layers deposited in midair.

The measurement process was carried out using the GOM ATOS optical measurement system following post-processing steps. Initially, the 3D-printed cutting edges were digitized in their as-printed state (referred to as the 0-state) to serve as reference data. Afterward, three sheets were cut, followed by a second round of scanning. Subsequently, an additional three sheets were cut, and the process concluded with a third round of measurement.

Thus, each test specimen involved six cutting operations. This six-cut sequence was conducted for both 0.22 mm and 0.3 mm thick sheets. The process is illustrated in Figure 6, and the press assembly is shown in Figure 7.

Figure 6. Flowchart of the scanning process.

Figure 7. Measuring set-up. (One active tool (white). The metal parts are included in the machine: D80 mm, D100 mm, D250 mm, and some rubber sheets are visible above the active tool).

The evaluation of measurement results was performed using ATOS 2017 software. The 0-state served as the reference (nominal data), and subsequent measurement states were compared to this reference using best-fit alignment. This method, widely used in both industrial and research applications, aligns data to the most optimal fit when no specific orientation is prescribed.

During the measurements, signs of wear or worn cutting edge sections were assessed at four characteristic locations, as depicted in Figure 8. Additionally, color-mapped analysis was employed to examine further geometric changes in the cutting edges.

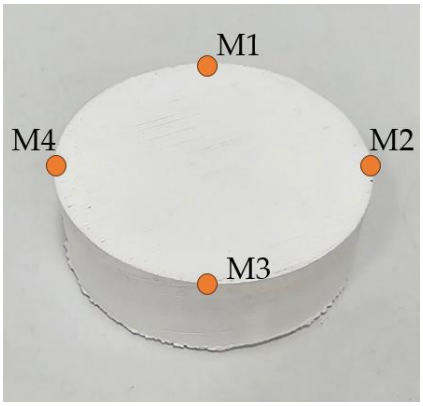

Figure 8. Measuring points.

In summary, the evaluation and analysis of the study were as follows: The tool elements used for cutting were 3D scanned according to the measurement flow chart, where the authors examined their dimensional changes, possible cracks, or even complete stamping. Successfully cut specimens were visually inspected for their tendency to warp according to the evaluation scheme given below. Since Komarov tools [48] were used to clamp the shape of the tool onto the specimen, their needle spacing was the same as that of the tools. For this small number of test pieces, it was not necessary to specify a separate tolerance class for the tools, so the tolerance class expected for the workpieces was obtained.

Naturally, the authors will carry out measurements with a larger number of pieces in their next experiment based on the results of this experiment.

3. Results and Discussion

To conduct the investigations, 2 × 3 sets of tools (1 set = 9 pieces) were printed, resulting in a total of 2 × 27 cutting edges. Three sets were designed for cutting 0.22 mm thick Al99.5 H24 sheets and three for 0.3 mm thick sheets. Each tool performed six cuts, and after every three cuts, the tools were scanned (as outlined in the process diagram) to determine the extent of tool wear. The total number of cuts needed to carry out the experiment was, therefore, 54 × 6, or 324.

As anticipated, some tools failed under the applied load, sometimes breaking during the very first cut. One such failed tool is shown in Figure 9.

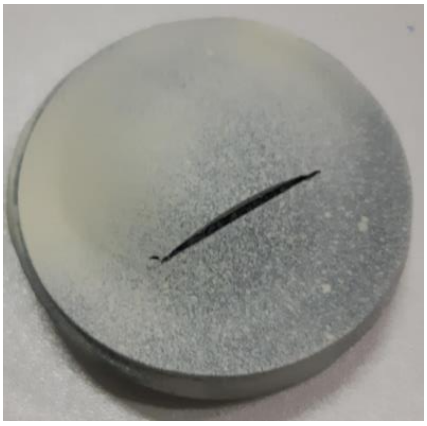

Figure 9. Deformed cutting edges.

The experimental results demonstrated that most tools performed well; however, certain cutting edges experienced significant deformation or fracture during the cutting process. This issue was particularly evident in tools A1 and B1, which were printed with a 2 mm wall thickness and oriented at 0° or 15°.

Burr formation was also examined visually during the tests. The degree of burr formation was categorized as minimal when barely noticeable by touch, with a burr thickness of 0.01–0.05 mm; as moderate when clearly noticeable by touch but not necessarily requiring post-processing, with a burr thickness of 0.05–0.1 mm; and as severe when the burrs were sharp, easily visible, and potentially hazardous, exceeding a thickness of 0.1 mm.

In many cases, the cut workpieces exhibited high-quality contours. Burr formation was either absent or minimal for several tools. In some instances, however, minimal to moderate burr formation was observed, likely influenced by human factors during the pressing process. Minor positional variations in the tool system during each pressing cycle, as well as slight shifts in the relative positions of the sheet, rubber pads, and pressing element, may have contributed to this outcome.

For tools manufactured using FDM technology with PLA material, seven out of nine tool designs successfully completed all six cuts on 0.22 mm thick Al99.5 sheets. Exceptions included models A1 and A2, which displayed significant deformation and cracking after the third cut, rendering them unsuitable for further operations. Figure 10 compares the cutting edges of models A1 and A2 after three cuts with their initial state.

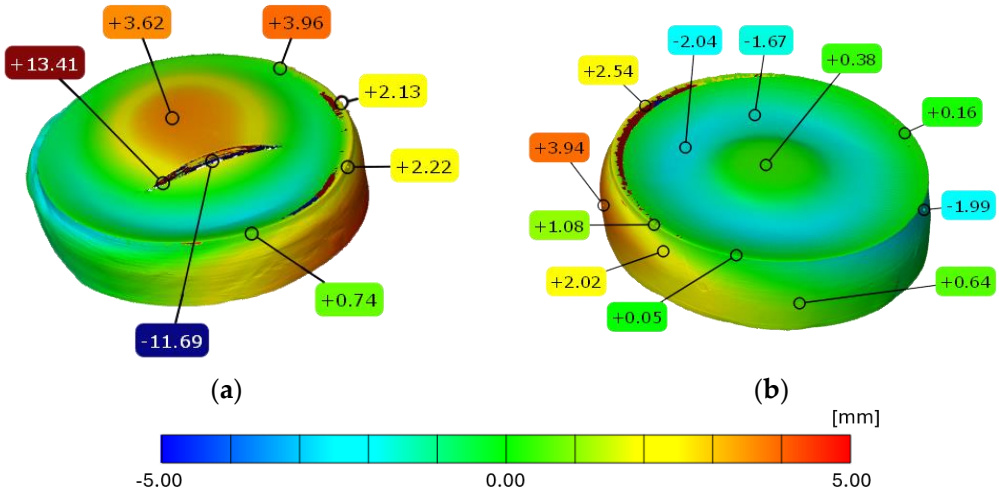

Figure 10. Edge wear values for models: (**a**) A1 and (**b**) A2—0.22 mm thick Al99.5 sheets.

During the evaluation, the initial and post-sixth pressing states were compared using GOM software. After aligning the models, color maps generated by the software highlighted differences between them. By placing measurement points on the models, these deviations could also be quantified numerically. For the seven cutting edges that successfully completed all six cuts, the average edge wear was in the range of hundredths of a millimeter, with values ranging from –0.05 mm to +0.04 mm. These measurements align with the IT9-IT10 tolerance class (ISO 286-1) [51], which is considered acceptable for this technology. Among the seven models, almost all performed well, but the A3 and C3 models stood out, with average deviations not exceeding 0.04 mm. Detailed evaluation results for the C3 model are shown in Figure 11.

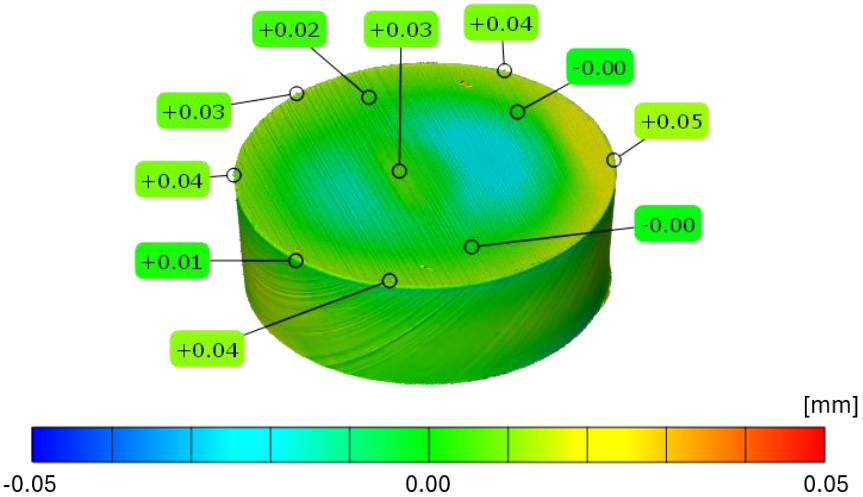

Figure 11. Edge wear values for model C3—0.22 mm thick Al99.5 sheets.

Beyond the color-mapped tool analysis, the cut workpieces were also examined, focusing primarily on burr formation. For the well-performing tools, minimal burr formation was observed in every case. An example of a successful cut using a 0.22 mm thick sheet is shown in Figure 12.

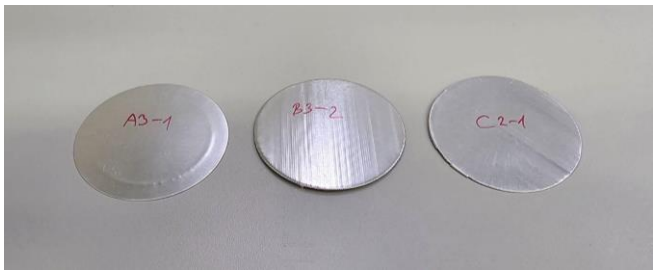

Figure 12. Examples of successful cuts—0.22 mm thick Al99.5 sheets.

Evaluation of the 0.3 mm thick Al99.5 sheets was carried out similarly to the thinner sheets. However, cutting the thicker 0.3 mm sheets proved less successful. Tools A1, A2, B1, and C1 were unable to complete all six cuts, as they suffered significant deformation during the process and were unsuitable for further use. This outcome was partly expected since the 0.3 mm sheet falls more into the category of fine sheets rather than thin sheets, as illustrated in Figure 13.

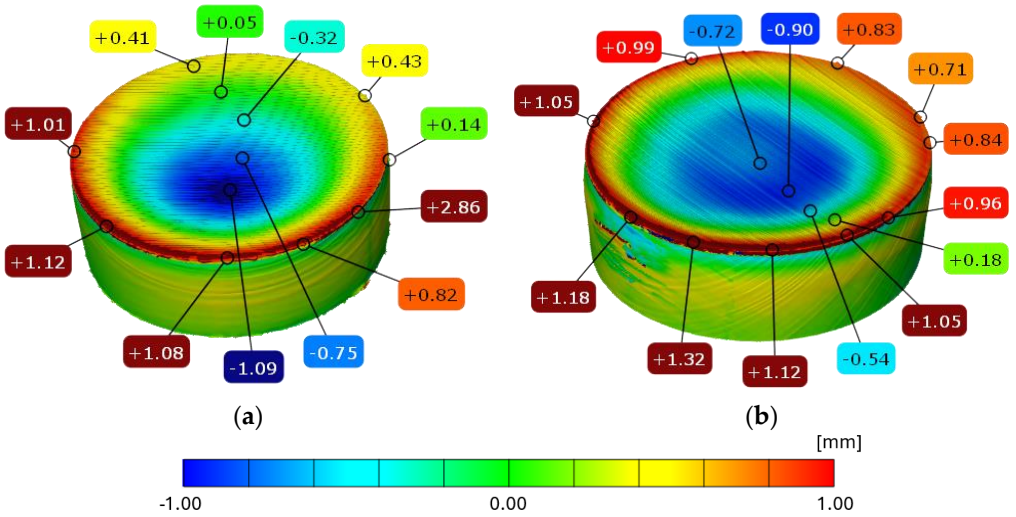

Figure 13. Edge wear values for models: (**a**) B1 and (**b**) C1—0.3 mm thick Al99.5 sheets.

Overall, the A3 model performed the best, with near-zero average wear and minimal deviations that ranged between −0.01 mm and +0.01 mm, as shown in Figure 14.

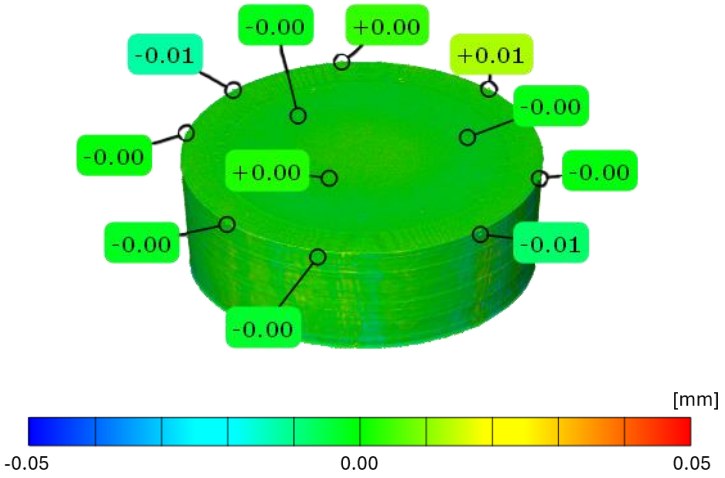

Figure 14. Edge wear values for model A3—0.3 mm thick Al99.5 sheets.

In contrast, the poorest performance was observed from the C2 cutting edge. As depicted in Figure 15, the tool not only deformed but also tore the sheet during operation.

Figure 15. An example of an unsuccessful cut—0.3 mm thick Al99.5 sheets.

Examples of successful cuts with minimal burr formation are presented in Figure 16. The observed burr formation was on the borderline between minimal and moderate, which is considered acceptable in practice and represents a strong result for a 3D-printed tool.

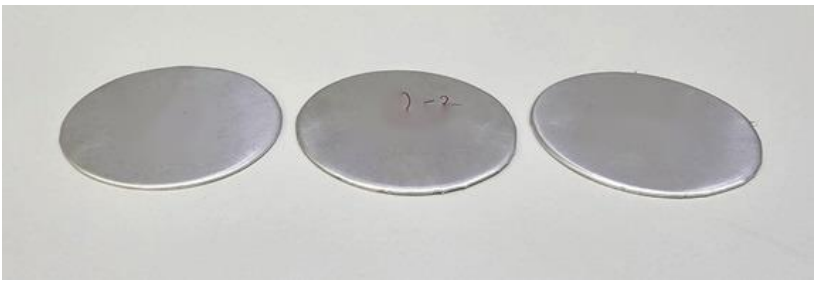

Figure 16. Examples of successful cuts—0.3 mm thick Al99.5 sheets.

For greater clarity, the results have been summarized in separate tables for each sheet thickness. The values shown in Tables 10 and 11 represent the averages from three measurements. The tables show the average values only because it is an easier way to present the results.

Table 10. Edge wear following the cutting of 0.22 mm thick Al99.5 sheets in mm (M1–M4 points are in accordance with Figure 8).

Model	Orientation	Wall Thickness [mm]	M1	M2	M3	M4
A1	0°	2	-	-	-	-
A2	0°	4	-	-	-	-
A3	0°	6	0.02	0.00	0.01	0.01
B1	15°	2	0.00	0.02	−0.01	−0.04
B2	15°	4	−0.09	−0.03	−0.04	−0.03
B3	15°	6	−0.05	−0.01	−0.03	−0.03
C1	45°	2	0.01	0.04	0.03	0.04
C2	45°	4	0.00	−0.01	0.00	−0.02
C3	45°	6	0.00	0.01	0.00	0.01

Table 11. Edge wear following the cutting of 0.3 mm thick Al99.5 sheets in mm unit (M1–M4 points are in accordance with Figure 8).

Model	Orientation	Wall Thickness [mm]	M1	M2	M3	M4
A1	0°	2	-	-	-	-
A2	0°	4	-	-	-	-
A3	0°	6	0.00	0.00	–0.01	0.01
B1	15°	2	-	-	-	-
B2	15°	4	0.10	0.12	0.01	0.02
B3	15°	6	−0.02	−0.05	−0.07	0.00
C1	45°	2	-	-	-	-
C2	45°	4	0.47	0.42	0.48	0.40
C3	45°	6	0.04	0.03	0.04	0.06

4. Conclusions

This study established the feasibility and practicality of using FDM 3D printing technology to produce cutting tools for thin aluminum sheets, particularly for prototyping and small-scale production. The research highlights the following key findings:

Performance and design parameters:

- PLA-based tools successfully executed multiple cuts with minimal wear and acceptable burr formation, achieving industry-standard tolerances (IT9 and IT10);
- Tools with a 45° orientation and a 6 mm wall thickness demonstrated superior durability and wear resistance, emphasizing the importance of print orientation and wall thickness in tool design;
- Despite PLA not being recommended for cutting applications, it proved viable for low-stress tasks involving thin sheets.

Economic and time efficiency:

- Production costs were reduced by up to 90% compared to traditional machining methods.
- Lead times were shortened by 50–70%, underscoring the value of FDM technology in agile and cost-sensitive applications.

However, limitations were observed, particularly with the use of PLA for high-stress applications. Cutting thicker sheets (0.3 mm) posed challenges, leading to deformation and failure in some tool designs. These findings underline the necessity for further refinement in material selection and tool design.

Future research will aim to address these limitations and expand the applicability of FDM technology by focusing on the following:

- Material enhancements: integrating stronger composite materials to improve mechanical properties and performance under higher loads;
- Design optimization: leveraging advanced printing techniques and AI-driven design optimization [52–54] to enhance tool efficiency and reliability;
- Operational improvements: developing lubrication-free cutting processes to align with environmental sustainability and reduce friction-related failures.

By incorporating these advancements, FDM-printed tools have the potential to transition from prototyping applications to broader industrial uses, offering an innovative, cost-effective, and transformative solution for modern manufacturing.

Author Contributions: Conceptualization, S.S., B.F.S., V.N., G.S., D.K., M.S. and S.F.; methodology, S.S., B.F.S., V.N., G.S., D.K., M.S. and S.F.; software, S.S., B.F.S., V.N., G.S., D.K., M.S. and S.F.; validation, S.S., B.F.S., V.N., G.S., D.K., M.S. and S.F.; formal analysis, S.S., B.F.S., V.N., G.S., D.K., M.S. and S.F.; investigation, S.S., B.F.S., V.N., G.S., D.K., M.S. and S.F.; resources, S.S., B.F.S., V.N., G.S., D.K., M.S. and S.F.; data curation, S.S., B.F.S., V.N., G.S., D.K., M.S. and S.F.; writing—original draft

preparation, S.S., B.F.S., V.N., G.S., D.K., M.S. and S.F.; writing—review and editing, S.S., B.F.S., V.N., G.S., D.K., M.S. and S.F.; visualization, S.S., B.F.S., V.N., G.S., D.K., M.S. and S.F.; supervision, S.S., B.F.S., V.N., G.S., D.K., M.S. and S.F.; project administration, S.S., B.F.S., V.N., G.S., D.K., M.S. and S.F.; funding acquisition, S.S., B.F.S., V.N., G.S., D.K., M.S. and S.F. All authors have read and agreed to the published version of the manuscript.

Funding: This research received no external funding.

Institutional Review Board Statement: Not applicable.

Informed Consent Statement: Not applicable.

Data Availability Statement: All data are available within the paper.

Acknowledgments: This paper was written by the research team "SZE-RAIL".

Conflicts of Interest: The authors declare no conflicts of interest.

Abbreviations

3D	Three-dimensional
ABS	Acrylonitrile butadiene styrene
ASTM	American Society for Testing and Materials
CAD	Computer-aided design
DIC	Digital image correlation
DD	Dual drive
FDM	Fused deposition modeling
IT	International tolerance
ISO	International Organization for Standardization
PETG	Polyethylene terephthalate glycol-modified
PU	Polyurethane
TPU	Thermoplastic polyurethane
Nomenclature	
$A_{11.3}$	Percentage strain at breakage (related to a $L_o = 10 \cdot d_0$ measuring basis)
d_0	Original diameter or thickness of the sample/specimen before deformation
H	Cutting die height [mm]
s	Thickness of the sheet (plate) [mm]
α	Conical angle [°]

References

1. Klimyuk, D.; Serezhkin, M.; Plokhikh, A. Application of 3D Printing in Sheet Metal Forming. *Mater. Today Proc.* **2021**, *38*, 1579–1583. [CrossRef]
2. Tondini, F.; Basso, A.; Arinbjarnar, U.; Nielsen, C.V. The Performance of 3D Printed Polymer Tools in Sheet Metal Forming. *Metals* **2021**, *11*, 1256. [CrossRef]
3. Hattalli, V.L.; Srivatsa, S.R. Sheet Metal Forming Processes–Recent Technological Advances. *Mater. Today Proc.* **2018**, *5*, 2564–2574. [CrossRef]
4. Trzepieciński, T. Recent Developments and Trends in Sheet Metal Forming. *Metals* **2020**, *10*, 779. [CrossRef]
5. Blatnický, M.; Dižo, J.; Gerlici, J.; Sága, M.; Lack, T.; Kuba, E. Design of a Robotic Manipulator for Handling Products of Automotive Industry. *Int. J. Adv. Robot. Syst.* **2020**, *17*, 1729881420906290. [CrossRef]
6. Dižo, J.; Blatnický, M.; Sága, M.; Harušinec, J.; Gerlici, J.; Legutko, S. Development of a New System for Attaching the Wheels of the Front Axle in the Cross-Country Vehicle. *Symmetry* **2020**, *12*, 1156. [CrossRef]
7. Volkov, V.; Taran, I.; Volkova, T.; Pavlenko, O.; Berezhnaja, N. Determining the Efficient Management System for a Specialized Transport Enterprise. *Nauk. Visnyk Natsionalnoho Hirnychoho Universytetu* **2020**, *2020*, 185–191. [CrossRef]
8. Saukenova, I.; Oliskevych, M.; Taran, I.; Toktamyssova, A.; Aliakbarkyzy, D.; Pelo, R. Optimization of Schedules for Early Garbage Collection and Disposal in the Megapolis. *East.-Eur. J. Enterp. Technol.* **2022**, *1*, 13–23. [CrossRef]
9. Zaragoza, V.G.; Rane, K.; Strano, M.; Monno, M. Manufacturing and Performance of 3D Printed Plastic Tools for Air Bending Applications. *J. Manuf. Process.* **2021**, *66*, 460–469. [CrossRef]

10. Durgun, I. Sheet Metal Forming Using FDM Rapid Prototype Tool. *Rapid Prototyp. J.* **2015**, *21*, 412–422. [CrossRef]
11. Male, A.T.; Chen, Y.W.; Pan, C.; Zhang, Y.M. Rapid Prototyping of Sheet Metal Components by Plasma-Jet Forming. *J. Mater. Process. Technol.* **2003**, *135*, 340–346. [CrossRef]
12. Macdonald, E.; Salas, R.; Espalin, D.; Perez, M.; Aguilera, E.; Muse, D.; Wicker, R.B. 3D Printing for the Rapid Prototyping of Structural Electronics. *IEEE Access* **2014**, *2*, 234–242. [CrossRef]
13. Tondini, F.; Arinbjarnar, U.; Basso, A.; Nielsen, C.V. 3D printing to facilitate flexible sheet metal forming production. *Procedia CIRP* **2021**, *103*, 91–96. [CrossRef]
14. Fischer, S.; Harangozó, D.; Németh, D.; Kocsis, B.; Sysyn, M.; Kurhan, D.; Brautigam, A. Investigation of Heat-Affected Zones of Thermite Rail Welding. *Facta Univ. Ser. Mech. Eng.* **2024**, *22*, 689–710. [CrossRef]
15. Németh, A.; Fischer, S. Investigation of the Glued Insulated Rail Joints Applied to CWR Tracks. *Facta Univ. Ser. Mech. Eng.* **2021**, *19*, 681–704. [CrossRef]
16. Kuchak, A.T.J.; Marinkovic, D.; Zehn, M. Parametric Investigation of a Rail Damper Design Based on a Lab-Scaled Model. *J. Vib. Eng. Technol.* **2021**, *9*, 51–60. [CrossRef]
17. Kuchak, A.T.J.; Marinkovic, D.; Zehn, M. Finite Element Model Updating—Case Study of a Rail Damper. *Struct. Eng. Mech.* **2020**, *73*, 27–35. [CrossRef]
18. Nakamura, N.; Mori, K.-I.; Abe, Y. Applicability of Plastic Tools Additively Manufactured by Fused Deposition Modelling for Sheet Metal Forming. *Int. J. Adv. Manuf. Technol.* **2020**, *108*, 975–985. [CrossRef]
19. Zaragoza, V.G.; Strano, M.; Iorio, L.; Monno, M. Sheet Metal Bending with Flexible Tools. *Procedia Manuf.* **2019**, *32*, 232–239. [CrossRef]
20. Schuh, G.; Bergweiler, G.; Fiedler, F.; Bickendorf, P.; Colag, C. A Review on Flexible Forming of Sheet Metal Parts. In Proceedings of the 2019 IEEE International Conference on Industrial Engineering and Engineering Management (IEEM), Macao, China, 15−18 December 2019; pp. 1221–1225. [CrossRef]
21. Frohn-Sörensen, P.; Geueke, M.; Tuli, T.B.; Kuhnhen, C.; Manns, M.; Engel, B. 3D Printed Prototyping Tools for Flexible Sheet Metal Drawing. *Int. J. Adv. Manuf. Technol.* **2021**, *115*, 2623–2637. [CrossRef]
22. Orzeł, B.; Stecuła, K. Comparison of 3D Printout Quality from FDM and MSLA Technology in Unit Production. *Symmetry* **2022**, *14*, 910. [CrossRef]
23. Wong, K.V.; Hernandez, A. A Review of Additive Manufacturing. *ISRN Mech. Eng.* **2012**, *2012*, 208760. [CrossRef]
24. Wickramasinghe, S.; Do, T.; Tran, P. FDM-Based 3D Printing of Polymer and Associated Composite: A Review on Mechanical Properties, Defects and Treatments. *Polymers* **2020**, *12*, 1529. [CrossRef]
25. Szabó, B.; Pásthy, L.; Orosz, Á.; Tamás, K. The Investigation of Additive Manufacturing and Moldable Materials to Produce Railway Ballast Grain Analogs. *Frat. Integrità Strutt.* **2022**, *60*, 213–228. [CrossRef]
26. Ézsiás, L.; Tompa, R.; Fischer, S. Investigation of the Possible Correlations between Specific Characteristics of Crushed Stone Aggregates. *Spectr. Mech. Eng. Oper. Res.* **2024**, *1*, 10–26. [CrossRef]
27. Szalai, S.; Eller, B.; Juhász, E.; Movahedi, R.M.; Németh, A.; Harrach, D.; Baranyai, G.; Fischer, S. Investigation of Deformations of Ballasted Railway Track During Collapse Using the Digital Image Correlation Method (DICM). *Rep. Mech. Eng.* **2022**, *3*, 168–191. [CrossRef]
28. Fischer, S. Investigation of the Settlement Behavior of Ballasted Railway Tracks Due to Dynamic Loading. *Spectr. Mech. Eng. Oper. Res.* **2025**, *2*, 24–46. [CrossRef]
29. Yang, D.Y.; Bambach, M.; Cao, J.; Duflou, J.R.; Groche, P.; Kuboki, T.; Sterzing, A.; Tekkaya, A.E.; Lee, C.W. Flexibility in Metal Forming. *CIRP Ann.* **2018**, *67*, 743–765. [CrossRef]
30. Schuh, G.; Bergweiler, G.; Bickendorf, P.; Fiedler, F.; Colag, C. Sheet Metal Forming Using Additively Manufactured Polymer Tools. *Procedia CIRP* **2020**, *88*, 20–25. [CrossRef]
31. Nakamura, N.; Mori, K.-I.; Abe, F.; Abe, Y. Bending of Sheet Metals Using Plastic Tools Made with 3D Printer. *Procedia Manuf.* **2018**, *20*, 737–742. [CrossRef]
32. Belter, J.T.; Dollar, A.M. Strengthening of 3D Printed Fused Deposition Manufactured Parts Using the Fill Compositing Technique. *PLoS ONE* **2015**, *10*, e0122915. [CrossRef] [PubMed]
33. Baker, A.M.; Mccoy, J.O.H.N.; Majumdar, B.S.; Rumley-Ouellette, B.R.I.T.T.A.N.Y.; Wahry, J.A.C.O.B.; Marchi, A.N.; Bernardin, J.D.; Spernjak, D.U.S.A.N. Measurement and Modelling of Thermal and Mechanical Anisotropy of Parts Additively Manufactured Using Fused Deposition Modelling (FDM). In *Structural Health Monitoring*; DEStech Publications: Lancaster, PA, USA, 2017; pp. 612–620. [CrossRef]
34. Mohammad, A.M.J.A. Statistical-Based Optimization of Process Parameters of Fused Deposition Modelling for Improved Quality. Ph.D. Thesis, University of Nottingham, Nottingham, UK, 2012. Available online: https://pure.port.ac.uk/ws/portalfiles/portal/5315191/Thesis_PDF_Moh_ALHUBAIL.pdf (accessed on 29 November 2024).
35. Tuteski, O.; Kočov, A. Tensile Strength and Dimensional Variances in Parts Manufactured by SLA 3D Printing. *Industry 4.0* **2021**, *6*, 143–149.

36. Beniak, J.; Križan, P.; Šooš, M.; Matuš, M. Research on Shape and Dimensional Accuracy of FDM Produced Parts. *IOP Conf. Ser. Mater. Sci. Eng.* **2019**, *501*, 012030. [CrossRef]
37. Sudin, M.N.; Shamsudin, S.A.; Abdullah, M.A. Effect of Part Features on Dimensional Accuracy of FDM Model. *APRN J. Eng. Appl. Sci.* **2016**, *11*, 8067–8072.
38. Akbaş, O.E.; Hıra, O.; Hervan, S.Z.; Samankan, S.; Altınkaynak, A. Dimensional Accuracy of FDM-Printed Polymer Parts. *Rapid Prototyp. J.* **2020**, *26*, 288–298. [CrossRef]
39. Tong, K.; Joshi, S.; Lehtihet, E.A. Error Compensation for Fused Deposition Modeling (FDM) Machine by Correcting Slice Files. *Rapid Prototyp. J.* **2008**, *14*, 4–14. [CrossRef]
40. *ISO 209:2007*; Wrought Aluminium and Aluminium Alloys—Chemical Composition. ISO: Geneva, Switzerland, 2007.
41. *ISO 6892-1:2019*; Metallic Materials—Tensile Testing—Part 1: Method of Test at Room Temperature. ISO: Geneva, Switzerland, 2019.
42. *ISO 6506-4:2014*; Metallic Materials—Brinell Hardness Test—Part 4: Table of Hardness Values. ISO: Geneva, Switzerland, 2014.
43. *ASTM D792*; Standard Test Methods for Density and Specific Gravity (Relative Density) of Plastics by Displacement. ASTM International: West Conshohocken, PA, USA, 2020.
44. *ASTM D790*; Standard Test Methods for Flexural Properties of Unreinforced and Reinforced Plastics and Electrical Insulating Materials. ASTM International: West Conshohocken, PA, USA, 2020.
45. *ASTM D3418*; Standard Test Method for Transition Temperatures of Polymers by Differential Scanning Calorimetry. ASTM International: West Conshohocken, PA, USA, 2020.
46. *ISO 527-1:2019*; Plastics—Determination of Tensile Properties. ISO: Geneve, Switzerland, 2019.
47. *ISO 180:2019*; Plastics—Determination of Izod Impact Strength. ISO: Geneve, Switzerland, 2019.
48. Bacskó, A.; Gál, G. Gumiszerszámos Lemezmegmunkálás. In Proceedings of the Fiatal Műszakiak Tudományos Ülésszaka, Cluj, Romania, 21–22 March 1997.
49. Skriba, Z. *A Fémek Képlékeny Alakításának Technológiája*; Műszaki Könyvkiadó: Budapest, Hungary, 1976.
50. Végvári, F. Négyzetes Lyukasztás és Kivágás Poliuretán Párnával. In Proceedings of the Fiatal Műszakiak Tudományos Ülésszaka, Cluj, Romania, 26–27 March 2004.
51. *ISO 286-1:2010*; Geometrical Product Specifications (GPS)—ISO Code System for Tolerances on Linear Sizes. ISO: Geneve, Switzerland, 2010.
52. Ficzere, P. The Role of Artificial Intelligence in the Development of Rail Transport. *Cogn. Sustain.* **2023**, *2*. [CrossRef]
53. Zamfirache, I.A.; Precup, R.E.; Petriu, E.M. Q-Learning, Policy Iteration and Actor-Critic Reinforcement Learning Combined with Metaheuristic Algorithms in Servo System Control. *Facta Univ. Ser. Mech. Eng.* **2023**, *21*, 615–630. [CrossRef]
54. Nosonovsky, M.; Aglikov, A.S. Triboinformatics: Machine Learning Methods for Frictional Instabilities. *Facta Univ. Ser. Mech. Eng.* **2024**, *22*, 423–433. [CrossRef]